Behaviour of a ducted twin vertical axis turbine in a diversity of flow conditions

Martin Moreau, Grégory Germain, and Guillaume Maurice

***Abstract*—The tidal current flow conditions are complex, combining sheared velocity profiles, directional variability, turbulence and fluctuations due to the surface waves. To better understand the effect of these flow conditions on the turbine behaviour, we tested a 1/20 scale model of *HydroQuest*'s 1 MW-rated ducted twin vertical axis tidal turbine (2-VATT) in many experimental flow conditions. The controlled environment of the Ifremer's wave and current tank allows to study separately the effect of each flow characteristics. Overall, the results show that idealised experimental flow conditions are sufficient to asses the 2-VATT average power performance with an appropriate reference velocity choice. However, the whole flow complexity must be considered for an optimised mechanical structure design in terms of extreme and fatigue loads ensuring the turbine integrity over its life time. Comparison between the experimental results at reduced-scale and the full-scale results at sea still needs to be undertaken to continue improving the power performance prediction and the structure design method.**

***Index Terms*—Tidal current, Shear, Misalignment, Turbulence, Waves**

I. Introduction

OVER the past decade, several demonstrators have been tested around the world to harness the tidal stream energy [1]. In the locations identified for tidal energy projects, like the Paimpol-Bréhat (PB) test site, France, where *HydroQuest* tested its 1 MW-rated ducted twin vertical axis tidal turbine (2-VATT) demonstrator [2], the flow conditions are complex and combine multiple characteristics. This flow complexity is made of vertically sheared velocity profiles [3] with about 20 % velocity difference between the top and the bottom of the 2-VATT capture area at PB. In addition, the current direction varies between ebb and flood tides and over time [4]. The average ebb and flood tide directions at PB are asymmetrical with about 22° difference, so the 2-VATT operated with 7° and 15° misalignment angles between its heading and the flood and ebb tide directions respectively. The ambient turbulence adds to the tidal current complexity, with eventually bathymetry-generated vortices [5]; and surface waves cause velocity fluctuations in the water column [6]. At PB, the turbulence intensity is about 15 % for average velocities over 1 m.s^{-1} and the 2-VATT demonstrator faced severe sea conditions with wave heights up to about 6 m and peak periods up to 17 s.

Fig. 1. Ducted 2-VATT in the Flood tide Configuration in the Ifremer wave and current tank, with the 3 Components LDV probe upstream.

Predicting accurately the influence of these flow conditions on the tidal turbines power generation and mechanical loads is crucial for a cost effective design. Numerous experimental studies addressed the effect of the above mentioned flow conditions on horizontal axis tidal turbines (HATT) at reduced scale [7]–[10]. However, only a few considered vertical axis turbines in complex flow conditions, and most of them were dedicated to wind turbine applications [11], [12].

To better understand separately the effect of the flow shear, the turbine misalignment with the flow direction, the bathymetry-generated turbulence and the presence of surface waves on the behaviour of a ducted 2-VATT, we tested a 1/20 scale model of *HydroQuest*'s 1 MW-rated demonstrator in the Ifremer's wave and current tank in all these flow conditions (Fig. 1) [13]–[16]. The present paper intends to draw a synthesis of the tested experimental conditions (section II) and of the results in terms of power generation (section III-A) and structural loads (section III-B) to identify the critical conditions from a design point of view.

II. Material and method

A. Turbine model

The model is a 1/20 scale ducted 2-VATT geometrically similar to the 1 MW-rated demonstrator tested by *HydroQuest* at PB from 2019 to 2021 [2]. It is composed of two independent counter-rotating vertical axis rotor columns. Each column is made of two levels of H-type rotors with a 60° phase difference between the levels. Besides, each rotor of radius $R = D/2 = 200$ mm is made of $N = 3$ blades that are $H_{blade} = 190$ mm high with a chord c of 73 mm. Thus, the rotor

This work was financially supported in part by the French Research and Technology National Association (ANRT) under the convention Cifre n°2020/0688.

M. Moreau is at HydroQuest SAS, 16 chemin de Malacher, 38240 Meylan, and at the French Research Institute for Exploitation of the Sea (Ifremer), 62200 Boulogne-sur-Mer, France. (e-mail: martin.moreau@ifremer.fr).

G. Germain is at the French Research Institute for Exploitation of the Sea (Ifremer), 62200 Boulogne-sur-Mer, France. (e-mail: gregory.germain@ifremer.fr).

G. Maurice is at HydroQuest SAS, 16 chemin de Malacher, 38240 Meylan, France. (e-mail: guillaume.maurice@hydroquest.net).

Digital Object Identifier:
https://doi.org/10.36688/ewtec-2023-322

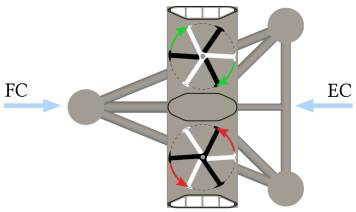

Fig. 2. Schematic top view of the ducted 2-VATT with the two flow configurations representing Flood and Ebb tide Configurations.

solidity (Nc/R) is 1.1. The rotors are mounted in a W = 1.24 m wide structure made of fairings and plates. The turbine height is defined as the distance between the top and the bottom horizontal plates such that H = 450 mm; and the 2-VATT capture area is $H \times W$. For this study, the turbine is fixed on a tripod bottom-mounted base similar to the demonstrator's one. The embedded instrumentation provides the torque Q and the rotational speed ω of each rotor column, the 6 load components applied between the turbine and the base as well as the 6 loads on the whole device including the base. All these signals are acquired at a sampling frequency of 128 Hz. The model and its instrumentation are fully described in [13].

Whether the flow comes from one side or the other of the device, the base geometry upstream and the relative counter-rotation direction of the two column reverses. The two flow directions are referred to either as FC, corresponding to the Flood tide Configuration at Paimpol-Bréhat test site, or as EC for the Ebb tide Configuration (Fig. 2).

B. Test cases and experimental setup

The ducted 2-VATT was tested in many configurations to assess independently the effect of the flow direction, the vertical shear, the bathymetry-generated turbulence and the surface waves on its behaviour. The scheme in Fig. 3 displays all the elements used to model these conditions in the Ifremer's 2 m deep (H_w) wave and current tank [17] and to measure the 2-VATT response, although they were never tested simultaneously altogether. The orthogonal coordinates system (x, y, z) is fixed with x pointing downstream and z towards the free surface and with x=0 at the 2-VATT centre.

To assess the effect of the flow direction and of the shear in steady flows, the wave-related apparatus and the bathymetry obstacles were absent from the experimental setup. With a homogeneous grid (G0) at the inlet, we can generate a uniform velocity field over the turbine capture area whereas with a variable grid porosity over the tank height (G1), we manage to generate a vertically sheared incident flow. Those grid arrangements are described in [7], [14]. We tested the 2-VATT in FC and EC with both G0 and G1. The turbine was also tested with $\pm$7° and $\pm$15° relative misalignment angles (α) between its heading and the flow direction, both around the reference FC and EC at α=0°. In all these configurations, the tank operated at a current velocity set point of 1 m.s^{-1}. The far upstream velocity was measured by the 2 Components Laser Doppler Velocimeter (2C-LDV) at $x = -6H$, at the centre of the projected capture area, ie. $(y, z) = (0, 0.505)$ m. That upstream distance was found to be outside the 2-VATT induction zone [13]. The power weighted average of the streamwise velocity at this position is noted U_0 and is considered as the reference velocity for the hydrodynamic coefficients computation. Using the same experimental setup, we also tested the 2-VATT at variable velocity set points between 0.8 and 1.8 m.s^{-1} with G0 and α=0° to assess the effect of the Reynolds number.

In addition, we tested the effect of surface waves on the behaviour of the ducted 2-VATT in wave-current conditions similar to those met at Paimpol-Bréhat test site [2]. Waves propagating against the current were tested with the turbine in EC and waves following the current were tested with the turbine in FC. In the first configuration, the wave maker is placed downstream the test section and the wave absorber downstream (like in Fig. 3), and vice versa for the following waves. A wave gauge was placed above the 2-VATT to measure the free surface elevation (η) and the 2C-LDV was placed at the same position upstream as in steady flows to measure the far upstream velocity synchronously with the 2-VATT related signals. The inlet was conditioned with the homogeneous grid G0 and the current velocity set point was 0.8 m.s^{-1}, which is the maximum capacity when generating surface waves. The 2-VATT was tested facing many wave conditions (Fig. 4) to assess the effect of the waves' amplitude and frequency in regular waves. The effect of irregular waves following a Jonswap spectrum compared to that of regular waves with similar significant wave height ($H_{1/3} = 2A_{1/3}$) and peak frequency (f_η, or period Tp) was also considered. Due to the wave-current interaction, the waves following the current are limited to quite low periods while the waves against current match the full-scale conditions according to the Froude similitude with a geometric scale factor of 20. In the present study, we compare the turbine behaviour in the conditions where the wave absorber and wave maker are immersed but inactive ($f00A0$) to the regular wave case $f04A2$ propagating against the current with f_η = 0.4 Hz and $A_{1/3} \simeq 100$ mm and to the irregular waves with a Jonswap Spectrum (JS ag.) with similar peak frequency and significant amplitude.

Finally, we tested the ducted 2-VATT both in FC and EC with bathymetry obstacles placed on the tank bottom upstream while the inlet was conditioned with G0 [15], [18]. Two obstacle combinations were considered: either a single square cylinder of base $h \times h$ and width $6h$, with h = 250 mm, referred to as C6, or a combination of that square cylinder with a cube of side h placed $2h$ upstream C6 at the centre of the tank, referred to as C1C6. A relative distance of $10h$ and $16h$ between the C6 centre and the 2-VATT centre was tested for both C6 and C1C6. In that experimental setup, unlike the previous ones, the 2C-LDV (and the 3C-LDV) was placed at $x = -1H$, right in front of the 2-VATT to measure simultaneously the current velocity fluctuations and the turbine response. The

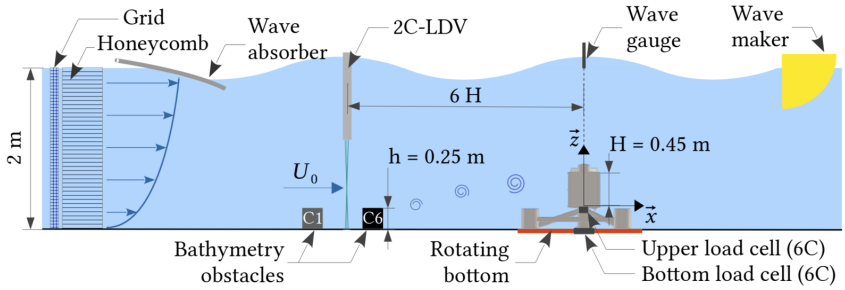

Fig. 3. Scheme of all the experimental setups gathered. Depending on the test cases, the wave maker and absorber, the bathymetry obstacles and the 2C-LDV could be removed.

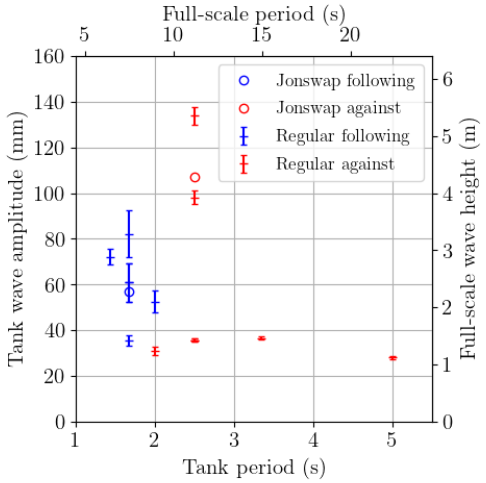

Fig. 4. Amplitude and period of the waves measured above the 2-VATT (left and bottom axes). The crosses with error bars represent the regular wave cases (average and standard deviation of the amplitude of the Hilbert transform of the free surface displacement) and the circle represent the JONSWAP cases ($A_{1/3}$, Tp). The right and top axes provide the waves period and height at a 20/1 scale according to Froude similitude law.

TABLE I
FLOW CONFIGURATION ABBREVIATIONS AND SYMBOLS.

Name	Description
EC	Ebb tide Configuration (Fig. 2)
FC	Flood tide Configuration (Fig. 2)
G0	Homogeneous grid providing a uniform velocity field
G1	Grid arrangement providing a vertically sheared velocity field
α	Relative angle between the flow direction and the 2-VATT heading
$f00A0$	G0 with the wave absorber and wave maker immersed for waves against current but inactive, in EC
$f04A2$	Regular waves propagating against the current (f_η = 0.4 Hz, $A_{1/3} \simeq$ 100 mm), in EC
JS ag.	Waves with a Jonswap Spectrum propagating against the current (f_η = 0.4 Hz, $A_{1/3} \simeq$ 110 mm), in EC
JS fo.	Waves with a Jonswap Spectrum following the current (f_η = 0.6 Hz, $A_{1/3} \simeq$ 60 mm), in FC
C6	Wide bathymetry obstacle ($h \times 6h \times h$) placed either at (@) 10 or 16h upstream the 2-VATT
C1C6	Combined bathymetry obstacles ($h \times h \times h$ in front of $h \times 6h \times h$) either at (@) 10 or 16h upstream the 2-VATT

tank operated at a current velocity set point of 1 m.s^{-1}, similarly to the reference cases in steady flow.

The abbreviations used to refer to either one or the other of the flow configurations are synthesised in Table I. In the following, when not specified, the grid in front of the honeycomb is the homogeneous one (G0) and the relative angle between the flow and the 2-VATT heading (α) is 0°.

C. Flow conditions

To provide an overview of the flow conditions in all the test cases mentioned before, Fig. 5 shows the streamwise average velocity and turbulence intensity in G0, G1, $f00A0$ and C6@10h. It appears that the average velocity profile is uniform over the 2-VATT height in G0 and in $f00A0$ with a low level of turbulence intensity (below 2 %). Note that the streamwise velocity profiles are similar to $f00A0$ over the 2-VATT capture height when surface waves are generated [19]. G1 provides a sheared average velocity profile that follows a power law similar to those at sea $\left(\overline{u}(z) = 1.2\,(z/H_w)^{1/7.9}\right)$ [3] with a low level of turbulence intensity, like the two previous conditions. With G0, G1 and waves, the flow conditions are homogeneous over the tank width with negligible transverse velocities. However, with bathymetry obstacles upstream, the flow characteristics are fully 3 dimensional with significant transverse velocities. In Fig. 5, a single profile is displayed at $y = W/4$, the lateral position of the rotor axis, to highlight the strong average velocity shear and turbulence intensity over the turbine height. Another important feature of the flow past the bathymetry obstacles is the presence of coherent flow structures at a shedding frequency about 0.25 Hz with a characteristic size of the order of W/2 in the wake of C6 [15]. Full description of the flow characteristics in G0 can be found in [20], in [7] for G1 and in [19] for the wave cases. The flow past C6 and C1C6 bathymetry obstacles are presented in [21], [22].

The knowledge of the streamwise velocity distribution is also of interest to explain the loads distribution later on (Fig. 6). In G0 and G1 like in $f00A0$, the PDF is centred on the average velocity U_0 with a single mode and a narrow velocity range. With regular waves, the velocity range is increased due to the orbital velocities and the PDF shows 2 modes due to the periodicity of the flow fluctuations. The amplitude of the orbital velocity is about $0.09U_0$ in $f04A2$. With irregular waves, the PDF is centred on U_0 again, with a

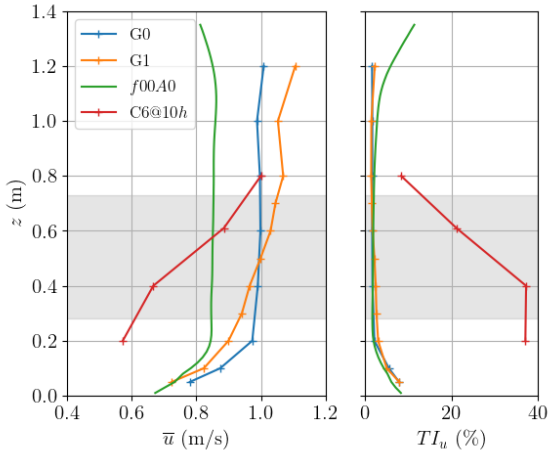

Fig. 5. Vertical profiles of the average streamwise velocity (left) and turbulence intensity (right) at the 2-VATT location. G0, G1 and C6 are 3C-LDV measurements whereas $f00A0$ is PIV from [19]. C6 profile is at $y = W/4$ (rotor axis lateral position), the others are at $y = 0$. The grey shade represents the 2-VATT capture height.

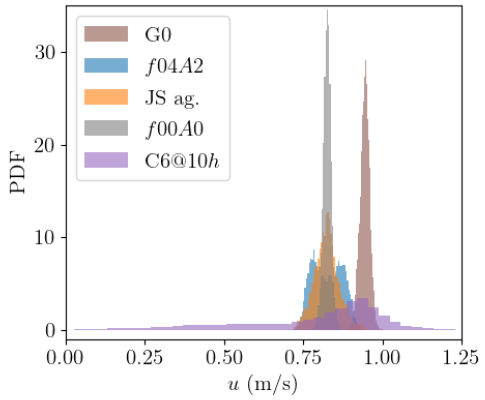

Fig. 6. Probability Density Function (PDF) of the streamwise velocity measured with the 2C-LDV at $(x, y, z) = (-6H, 0, 0.505\text{m})$ in front of the 2-VATT except for C6@10h whose measurement is with the 3C-LDV prior the turbine installation at $(x, y, z) = (-1H, 0, 0.610\text{m})$.

velocity range that slightly exceeds that of the regular wave case. Finally, the velocity distribution in the wake of the bathymetry obstacle C6 shows a single mode at U_0 and a wide velocity range with a low PDF due to the turbulence in the obstacle's wake.

D. Data processing

The performance results are analysed looking at the evolution of the power coefficient with the tip speed ratio (λ, (1)). λ_{opt} refers to the operating point providing the maximal power coefficient. The power coefficient of each rotor column C_{Pcol} is computed as in (2) with $P_{col}(t) = Q(t)\omega(t)$ and t the time. The reference surface is that of the rotors projected area and the torque signal considered are corrected by the friction torque induced by the seals and the transmission system for each rotor column [13]. Then, the overall average power coefficient $\overline{C_P}$ is the average of the two $C_{Pcol}(t)$ and the power fluctuations are analysed considering the average standard deviation between the two rotor columns, noted $\overline{\sigma}(C_{Pcol})$.

$$\lambda(t) = \frac{\omega(t)R}{U_0} \tag{1}$$

$$C_{Pcol}(t) = \frac{P_{col}(t)}{\rho D H_{blade} U_0^3} \tag{2}$$

The distribution of the torque coefficient (C_Q, (3)) along the rotor angular position of the green column (Fig. 2) is also analysed. The instantaneous relative angular position is computed by Hilbert transform of the torque signal filtered around the rotational frequency (f_ω). The angular position being relative, the absolute angle values displayed cannot be compared between graphs.

$$C_Q(t) = \frac{Q(t)}{\rho D H_{blade} R U_0^2} \tag{3}$$

The loads are analysed in the orthogonal coordinates system (x^*, y^*, z) rotating around z with the 2-VATT when $\alpha \neq 0°$, with x^* the turbine heading pointing downstream. The force and moment coefficients are defined by (4) and (5) for the components along x^* with the four rotors projected area as a reference surface. They are defined the same way for the loads along y^* and z. The loads measured without current are subtracted to consider only the hydrodynamic loads on the device. We consider the forces applied by the turbine on the gravity base, measured by the upper load cell, and the moments measured at the bottom (Fig. 3). The load probability density functions (PDF) are computed with 50 equal-width bins to consider the loads repartition and look at their extrema.

$$C_{x^*}(t) = \frac{F_{x^*}(t)}{2\rho D H_{blade} U_0^2} \tag{4}$$

$$C_{Mx^*}(t) = \frac{M_x^*(t)}{2\rho R D H_{blade} U_0^2} \tag{5}$$

III. Results synthesis

A. Power generation

1) In steady flows: Without bathymetry-generated turbulence nor surface waves, we measured the evolution of the power performance of the 2-VATT whether it operates in FC or EC, facing a uniform or a sheared velocity profile, and with aligned or misaligned current directions with regard to the turbine heading. Fig. 7 reveals a slightly lower maximal average power coefficient, about 5 %, and a 0.1 lower λ_{opt} in EC than in FC. This result is completely due to the difference of relative counter-rotation direction between FC and EC, and not to the base geometrical asymmetry [13]. In the reference condition with aligned uniform flow, the power coefficient fluctuations are higher in EC than in FC mostly due to the base geometry as the flow accelerates around the base feet, which are in front of the bottom rotors in EC against in front of the central fairing in FC. As a consequence, a torque generation asymmetry occurs between the lower and the upper rotors in EC that leads to higher power coefficient fluctuations than in FC.

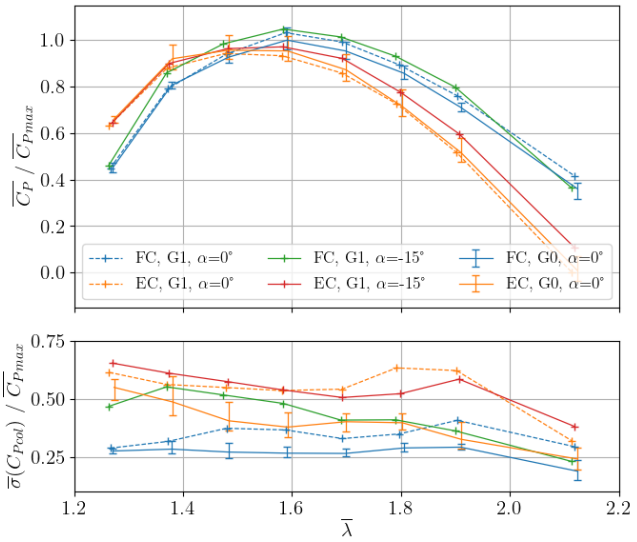

Fig. 7. Average (top) and standard deviation (bottom) of the power coefficients with regard to the tip speed ratio. The curves in the configuration G0 are averages over 3 test campaigns with the error bars representing the extreme average and extreme standard deviation values over the 3 campaigns. The C_P are normalised by the maximal average value in "FC, G0, α=0°".

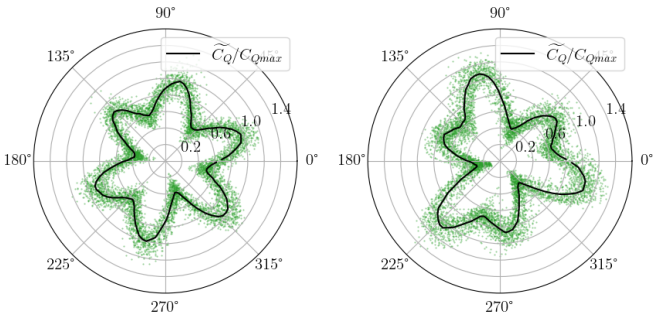

(a) G0 (b) G1

Fig. 8. Angular distribution of the green rotor column torque coefficient in FC with α=0° at λ_{opt}. The green dots are the instantaneous measurements and the black line is the phase average. The values are normalised by the maximal phase average value in G0. *Reminder*: the angular position is relative, so the absolute angle values cannot be compared between graphs.

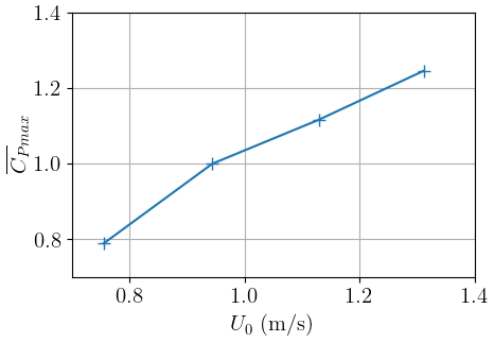

Fig. 9. Evolution of the normalised maximal average power coefficient with the far upstream average velocity measured by the 2C-LDV with the 2-VATT in FC, G0, α = 0°.

Besides, in the limits of the measurement repeatability, neither the velocity vertical shear nor the flow misalignment seem to affect the overall average power performance of the ducted 2-VATT. Looking in more details at the individual average power coefficient of each rotor column, an asymmetry appears between the two columns that grows with α [14]. This means that one rotor column is more loaded than the other one when operating with a misalignment angle. Furthermore, the power coefficient fluctuations are clearly higher when the flow is sheared compared to G0 with a $\overline{\sigma}(C_{Pcol})$ increase of 35 % both in FC and EC at λ_{opt}. That result can be explained looking at the torque distribution over the rotors angular position (Fig. 8). The distributions all show 6 torque maxima corresponding to the blades passing (one rotor column is composed of 2 times 3 bladed rotors). However, we can observe both amplitude asymmetry and different phase shift between the upper and the lower rotors, which is also indicated by a higher contribution of the peak at $3f_\omega$ relatively to that at $6f_\omega$ in the Fourier transform of the torque signal. With an incident vertically sheared flow, the upper rotors face higher velocity which generates a difference of both local tip speed ratio and available kinetic energy compared to the lower rotor, explaining the difference of torque angular distribution [14]. The flow misalignment also affects the torque angular distribution, in a different way whether the relative angle is positive or negative, but we lack absolute angular position measurement and local flow visualisation in the vicinity of the blades to explain that observation. Anyway, the average power coefficient asymmetry between the two rotor columns when operating at $\alpha \neq 0$ and the asymmetrical torque distribution between the upper and lower rotors when facing a sheared current must be taken into account in the extreme and fatigue load cases for an appropriate design of the rotor blades and shafts.

The two next parts are dedicated to the effect of unsteady flows, either in the wake of bathymetry obstacles or in presence of surface waves, on the power performance of the 2-VATT. Fig. 5 revealed that the average streamwise velocity is lower in these two configurations compared to the steady flow conditions. With $U_0 \simeq 1$ m.s^{-1}, the Reynolds number based on the blade chord and the rotational speed is about Re_c = 1 10^5 ((6) with λ = 1.5 and ν = 1.05 10^{-6} m^2.s^{-1} the water kinematic viscosity). Around this value, the foil lift and drag coefficients are dependent on the Reynolds number [23], and so does the rotor power performance [24]. Fig. 9 displays the evolution of the maximal average power coefficient with U_0 which shows about 20 % performance loss between U_0 = 1.0 and 0.8 m.s^{-1}. That Reynolds number effect must be taken into account for the experimental cases comparison.

$$Re_c = \frac{\lambda c U_0}{\nu} \tag{6}$$

2) In the wake of bathymetry obstacles: In a first approach, we compare the performance of the 2-VATT whether the bathymetry is flat or made of obstacles for a given far upstream velocity. We consider the same reference velocity value U_0 as in the reference case with G0 for all the cases since the tank operated at the same current velocity set point of 1 m.s^{-1}. Fig. 10 shows

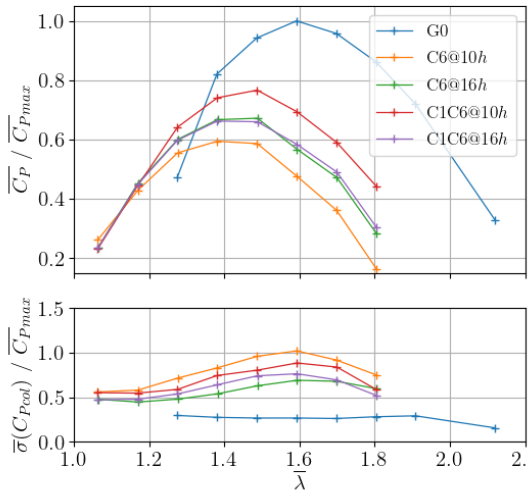

Fig. 10. Average and standard deviation of the power coefficient of the 2-VATT in FC at α = 0° in uniform steady flow and in the wake of the two combinations of bathymetry obstacles at two downstream distances. C_P are computed with the U_0 measured in G0 for all the cases and normalised by the maximal average value in G0.

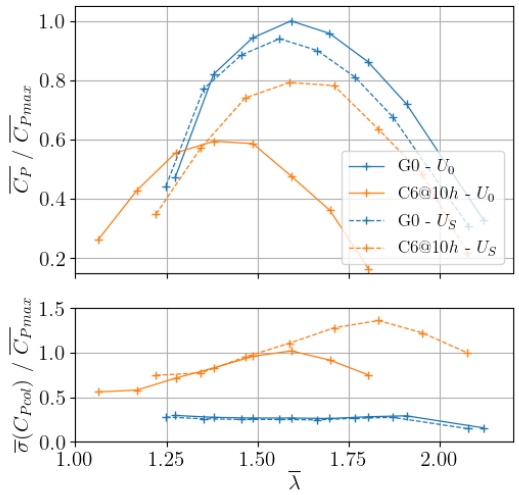

Fig. 11. Average and standard deviation of the power coefficient of the 2-VATT in FC at α = 0° in uniform steady flow and in the wake of C6. C_P are computed either with the U_0 measured in G0 for the two cases or with the velocity averaged over the 2-VATT capture area U_S measured at $x = -H$ without turbine. The values are normalised by the maximal average value in G0 with U_0.

the evolution of the average and standard deviation of the power coefficient of the 2-VATT in uniform steady flow versus in the wake of the two combinations of bathymetry obstacles at two downstream distances. Since the average velocity and kinetic energy really seen by the 2-VATT are lower in the wake of the bathymetry obstacles, the optimal tip speed ratio is lower and the maximal average power coefficient is lower too, up to 40 % in the worst condition tested with C6@10h. We notice an evolution of $\overline{C_P}$ with the distance to the obstacle that depends on the obstacle combination. Therefore, positioning tidal turbines in the most energetic areas of a specific tidal energy site at sea would require fine numerical simulations of the flow considering the local bathymetry [4].

Considering the power fluctuations, the sheared and turbulent flow in the wake of the bathymetry obstacles is responsible for up to 3 times higher $\overline{\sigma}(C_{Pcol})$ at λ_{opt} in the worst case compared to G0. Indeed, the Fourier transform of the torque signal reveals higher peak at $3f_\omega$ than at $6f_\omega$, which reveals a strong asymmetry between the two levels of rotors due to the sheared flow, as well as a peak at the coherent flow structures shedding frequency in the wake of C6 [15]. So, depending on the bathymetry roughness at the targeted tidal energy sites, rotors mechanical structure may need reinforced design regarding both extreme and fatigue loads.

When computing the power coefficients with the velocity averaged over the turbine capture area at the turbine location before its installation, noted U_S, in G0 and C6@10h, similarly to a resource assessment, λ_{opt} is found to be the same in the two conditions and also the same as with U_0 in G0 (Fig. 11). This result means that U_S is a good estimation of the velocity really perceived by the 2-VATT in operation. The average power coefficient remains 16 % lower in C6@10h compared to G0 when computed with U_S, which is a combined effect of the turbulent flow, whose velocity fluctuations increase the power weighted average, and of the difference of Reynolds number (Fig. 9) as U_S is 0.96 m.s^{-1} in G0 against 0.82 m.s^{-1} in C6@10h. From an operational point of view, these results highlight the impact of the reference velocity choice on the performance assessment results. The choice of the position of the velocity measurements at sea with regard to the bathymetry is therefore crucial for accurate performance assessment and monitoring of tidal turbines.

3) In presence of surface waves: Finally, we analyse the effect of surface waves propagating against the current on the performance of the ducted 2-VATT operating in EC (Fig. 12). When generating surface waves, both regular and irregular, the optimal tip speed ratio and the maximal average power coefficient appear unchanged compared to $f00A0$, with the wave maker and absorber immersed but inactive. However, the power coefficient standard deviation increases by about 50 % in the wave conditions considered here. We notice that regular and irregular waves of similar significant height and peak period affect the power coefficient average and fluctuations the same way. Considering the three regular wave conditions of variable amplitude at f_η = 0.4 Hz, we observe an increase of $\overline{\sigma}(C_{Pcol})$ quite linear with the wave amplitude [16]. In addition, in all the wave conditions tested, we observe peaks at the wave frequency and at frequencies combining the rotors rotational one and the wave one in the Fourier transform of the rotor column torque.

4) Synthesis: To sum up, first regarding the average performance and then the power fluctuations, we observe a ∼5 % lower optimal tip speed ratio and maximal power coefficient in EC than in FC, which should be taken into account for an optimised control law of such a ducted 2-VATT operating in tidal currents at sea. We find that neither the incident vertical shear, the relative flow misalignment up to 15° nor the presence of surface waves affect the overall maximal power coefficient and optimal tip speed ratio compared to the reference flow condition in G0 at α = 0°. This

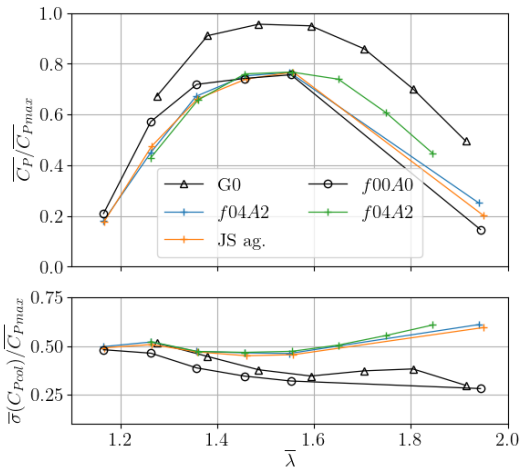

Fig. 12. Average and standard deviation of the power coefficient of the 2-VATT in EC at α = 0° in G0 with U_0 = 0.95 m.s^{-1} and in wave conditions with U_0 = 0.83 m.s^{-1}. The values are normalised by the maximal average value in "FC, G0, α=0°".

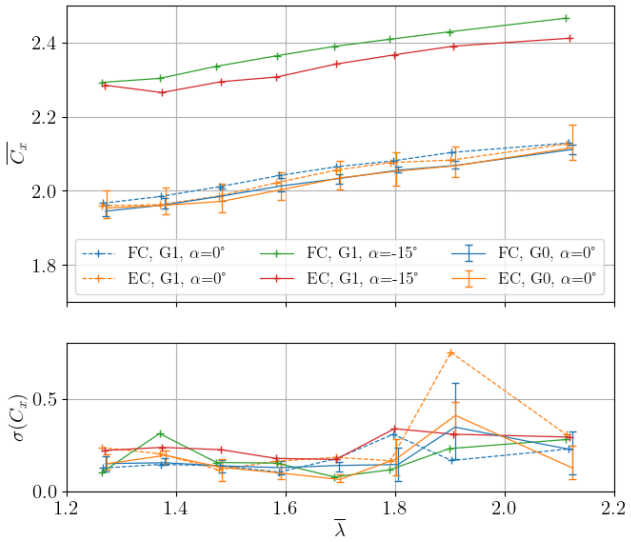

Fig. 13. Average (top) and standard deviation (bottom) of the drag coefficients with regard to the tip speed ratio. The curves in the configuration G0 are averages over 3 test campaigns with the error bars representing the extreme average and extreme standard deviation values over the 3 campaigns.

result means that experimental tests in idealised flow conditions can be sufficient to asses the average power performance of a ducted vertical axis tidal turbine. However, we also find that the flow misalignment causes a power generation asymmetry between the two rotor columns, meaning that the loads applied on a rotor column can be higher than expected when operating at $\alpha \neq 0°$. Finally, a rough bathymetry may generate severe velocity deficits locally compared to the theoretical potential of a given tidal energy site. That result must be considered carefully by tidal turbine developers both for turbine positioning to optimise the power output, and for velocity measurement positioning for correct power performance assessments and array monitoring.

Regarding the power fluctuations, we find that these are increased in all the tested flow conditions compared to the idealised flow condition with an aligned uniform flow in FC. A velocity shear over the turbine height, either present in the incident flow or due to the base geometry, generates real tip speed ratio and torque generation asymmetries between the upper and the lower rotors of a column that affects the angular torque distribution and increase the power fluctuations. The flow misalignment also affects the torque angular distribution but further analyses are needed to understand the underlying physics. The presence of large bathymetry obstacles upstream the 2-VATT is responsible for the strongest power fluctuations with a standard deviation of the power coefficient equal to its average. This is due to the strong velocity shear and to the coherent flow structures shed in the wake of such obstacles. These torque and power fluctuations must be considered at the turbine design stage for an appropriate structural design of the rotor columns and for electrical output power conditioning.

The next section focuses on the effect of the flow characteristics on the mechanical loads applied to the whole 2-VATT structure. For the structural design, key parameters are the extreme loads to ensure that the turbine will withstand extreme events without mechanical failure nor stability issue (sliding or overturning) and the load distributions for fatigue assessment to ensure the turbine integrity over its whole life time.

B. Mechanical loads

1) In steady flows: Fig. 13 shows the evolution of the drag coefficient with regard to the tip speed ratio whether the 2-VATT operates in FC or EC, in uniform or sheared flow, with or without misalignment. Typically, the streamwise force increases with λ, meaning that the extreme mechanical loads are likely to appear after a control failure causing the rotors to coast. Conversely to the power performance, we notice that the Reynolds number barely affects the 2-VATT loads as $\overline{C_x}$ rises by less than 5 % between U_0 = 0.76 and 1.69 m.s^{-1}. Regarding the flow conditions, the vertical shear does not affect the turbine drag but the relative heading misalignment strongly does with a 15 % increase of $\overline{C_x}$ when $\alpha = \pm 15°$. The drag fluctuations are not significantly affected by the vertical shear nor the misalignment. The $\sigma(C_x)$ variation around λ = 1.9 are not related to the flow conditions as it is rather related to a vibration mode of the model.

Independently from the flow conditions, the load fluctuations are affected by the relative rotor columns phasing, generating either one or two Probability Density Function (PDF) modes and affecting the load range on C_{x^*}, C_{y^*}, C_{Mx^*} and C_{My^*} [15]. The phased columns lead to the maximal range and value of C_{x^*} and C_{My^*} with two PDF modes and minima of C_{y^*} and C_{Mx^*} with one PDF mode. The rotor columns phase opposition leads to the contrary. Given the model control at constant rotational speed, the columns phasing is random at the rotation start but is kept the same during the test run. Conversely, the control of the full-scale demonstrator was more flexible so the columns phasing varied along time and the situation with rotors

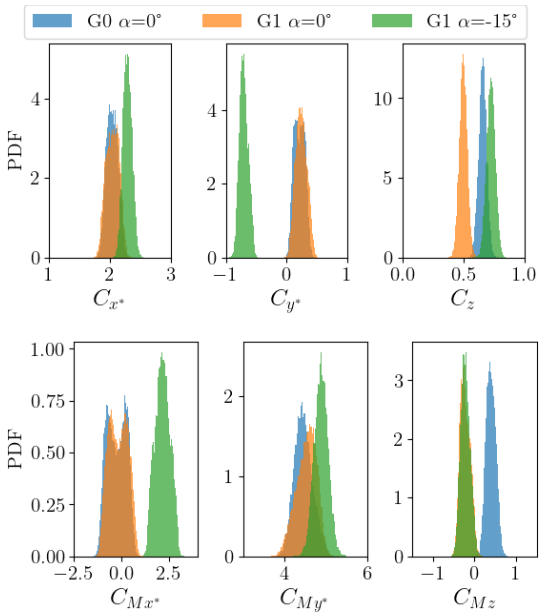

Fig. 14. Probability density functions of the 6 load components in the turbine coordinates system with the 2-VATT in FC in a uniform flow, a sheared flow and with a misalignment angle, close from λ_{opt}.

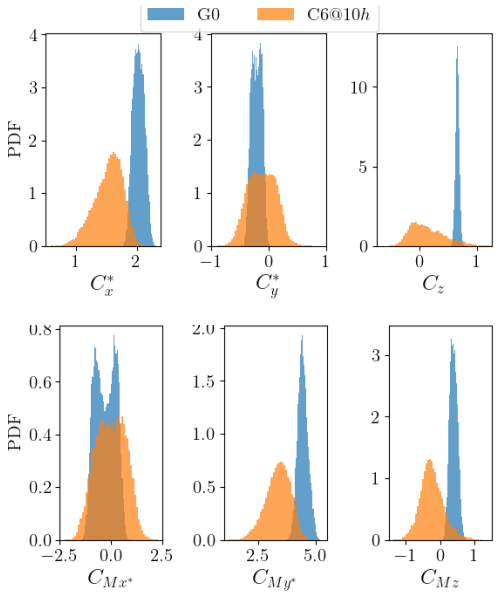

Fig. 15. Probability density functions of the 6 load components in the turbine coordinates system with the 2-VATT in FC with α = 0° in a uniform flow or in the wake of a bathymetry obstacle, close from λ_{opt}. The hydrodynamic coefficients are computed with U_0 in G0 for the two cases.

out of phase was the most likely. Thus, in the following, we compare the loads PDF with the 2-VATT operating at λ between 1.4 and 1.6 (around λ_{opt}) and with the rotor columns rather out of phase.

Fig. 14 displays the 6 load components PDF with the 2-VATT operating in FC in a uniform flow, a sheared flow and with a -15° misalignment angle. On one hand, we observe that the vertical shear only slightly affects the loads with a lower C_z that increases the vertical load downwards compared to the uniform flow and so reduces the device sliding risk. On the other hand, the turbine misalignment increases all the hydrodynamic coefficient extreme values (apart from C_{Mz}). The most impacted components are C_{y^*} and C_{Mx^*} whose extreme values are both about 2.5 times higher with α=-15° compared to 0°.

2) In the wake of bathymetry obstacles: Regarding the loads, we focus on the bathymetry obstacle configuration C6@10h which was found to be the most impacting condition on the power performance. Fig. 15 displays the 6 load components PDF in that configuration and in the reference condition G0, with the 2-VATT in FC at α = 0° for both. The presence of the bottom mounted obstacle leads to a ∼25 % drop of $\overline{C_{x^*}}$ and $\overline{C_{My^*}}$ computed with the far upstream velocity U_0 compared to G0 due to the decreased velocity in the wake of the bathymetry obstacle, similarly to the power coefficient. By contrast, computed with the surface averaged velocity at the 2-VATT location U_S, the values are of the same order of magnitude in G0 and in C6@10h, indicating no effect of the turbulence nor the flow shear on $\overline{C_{x^*}}$ and $\overline{C_{My^*}}$. Conversely, the vertical load $\overline{C_z}$ is more than 2.5 times lower in C6@10h compared to G0, independently from the reference velocity. This result means that the turbine apparent weight on the base is higher when the 2-VATT is in the wake of that bathymetry obstacle compared to the flat floor configuration, which contributes to the turbine stability. We explain this result by the negative vertical velocity field, up to $w = -0.1U_0$, measured in the wake of the bottom mounted cylinder near the turbine position [15].

Fig. 15 shows that, for all of the 6 load components, the range between the minimum and maximum values are significantly wider in C6@10h than in G0, which is due to the wider velocity range induced by the turbulence in the wake of the bathymetry obstacle. Indeed, the range between the first and the last percentile (p01 and p99 respectively) is 2.5 to 3.5 times higher in C6@10h for C_{x^*}, C_{y^*}, C_{My^*} and C_{Mz}, and up to 8.6 times higher for C_z. In addition the extreme p99 values are 1.3 to 1.6 times higher for the cross flow loads while the p99 C_{x^*} and C_{My^*} are 10 % lower in the wake of C6@10h than in G0 due to the average velocity deficit.

3) In presence of surface waves: Fig. 16 presents again the loads PDF, this time to compare the effect of regular and irregular surface waves propagating against the current on the 2-VATT behaviour operating in EC compared to the case without waves. By opposition to the load fluctuations induced by the turbulence on all the 6 components, the presence of surface waves only affects C_{x^*}, C_z and C_{My^*} while the three others are unchanged compared to the current only condition. Regarding the load components affected by the waves, we notice that the shape of their PDF is the same as that of the far upstream velocity, both with regular and irregular waves (Fig. 6), showing the strong correlation between the orbital velocity induced by the surface waves and the loads applied to the turbine. Indeed, the coherence function between the streamwise velocity measurement upstream and the load signals in the spectral domain is higher than 0.5 on the whole wave frequency range [16]. Besides, similarly to the power coefficient, we find that the standard deviations of the affected load components increase linearly with the

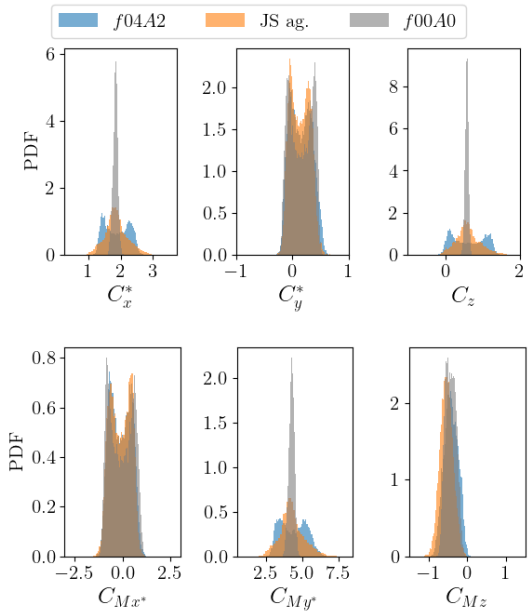

Fig. 16. Probability density functions of the 6 load components in the turbine coordinates system with the 2-VATT in EC with α = 0° subjected to waves propagating against the current, close from λ_{opt}.

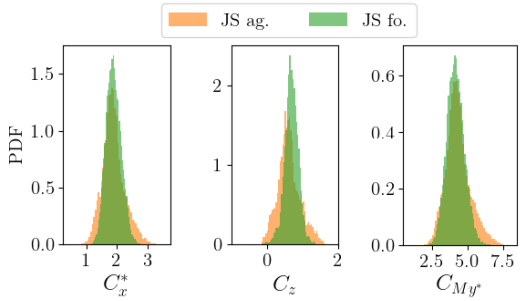

Fig. 17. Probability density functions of the 3 load components affected by the surface waves with the 2-VATT at α = 0° subjected to irregular waves either propagating against the current in EC or propagating with the current in FC. The rotors operate close from λ_{opt} with the two columns rather in phase.

wave amplitude in regular waves. When comparing the effect of regular and irregular waves of similar amplitude and period, it appears that both the loads extreme value and range are larger in irregular waves than in regular ones, although the C_{x^*} standard deviation is larger in $f04A2$ than in JS ag. due to the bimodal distribution. That bimodal PDF is specific to regular periodic waves and is not representative of the random wave conditions at sea. Therefore, when considering the effect of surface waves on the loads, the authors recommend conducting tests in irregular waves to get more realistic load distribution inputs for the turbine fatigue design.

Finally, Fig. 17 compares the PDF of the loads when the 2-VATT operates in irregular waves either in EC with waves opposing the current or in FC with waves following the current. The randomness of the rotor column phasing only gave test runs with rather phased columns in JS fo. around λ_{opt} so the PDF are compared in that situation for the two flow conditions. The wave amplitude is almost two times lower in JS fo. than in JS ag. (table I) and the wave period is smaller too,

TABLE II
LOADS EXTREME (THE ABSOLUTE VALUE OF P01 OR P99 WHETHER THE EXTREME VALUE IS NEGATIVE OR POSITIVE RESPECTIVELY) DEPENDING ON THE FLOW CONDITION, THE 2-VATT OPERATING CLOSE FROM λ_{opt} WITH ROTOR COLUMNS OUT OF PHASE.

Case	$C_x{}^*$	$C_y{}^*$	C_z	$C_{Mx}{}^*$	$C_{My}{}^*$	C_{Mz}
FC G0 α=0° (ref)	2.23	0.39	0.73	1.16	4.98	0.66
FC G1 α=0°	2.25	0.44	0.58	1.12	5.00	0.46
FC G1 α=-15°	2.54	0.87	0.81	2.63	5.67	0.42
FC C6@10h	1.98	0.63	0.94	1.53	4.42	0.96
EC JS ag.	2.79	0.47	1.48	1.08	6.47	0.91
max/ref	1.25	2.24	2.02	2.26	1.30	1.47

TABLE III
LOADS RANGE BETWEEN THE 1ST AND 99TH PERCENTILES, DEPENDING ON THE FLOW CONDITION, THE 2-VATT OPERATING CLOSE FROM λ_{opt} WITH ROTOR COLUMNS OUT OF PHASE.

Case	$C_x{}^*$	$C_y{}^*$	C_z	$C_{Mx}{}^*$	$C_{My}{}^*$	C_{Mz}
FC G0 α=0° (ref)	0.38	0.35	0.15	1.79	0.99	0.50
FC G1 α=0°	0.43	0.39	0.15	1.89	1.06	0.51
FC G1 α=-15°	0.59	0.25	0.16	0.82	1.71	0.42
FC C6@10h	1.06	1.03	1.31	2.98	2.43	1.69
EC JS ag.	1.71	0.64	1.52	1.91	3.92	0.76
max/ref	4.47	2.94	9.96	1.67	3.95	3.40

which results in smaller load range and extreme values applied to the 2-VATT. However, with surface waves of similar $H_{1/3}$ and Tp whether following or against the current, as it is the case between ebb and flood tides at sea, we expect stronger loads in the following wave case. Indeed, in that situation, the wave-current interaction stretches the wave length [6], which leads to bigger current velocity fluctuations in the whole water column due the wave orbital velocities.

4) Synthesis: To sum up regarding the effect of complex flow conditions on the loads applied to the ducted 2-VATT, we found first that the rotor columns phasing affects the load distributions. The most critical situations regarding the loads range and their extreme values are when the columns are perfectly either in phase or in phase opposition, for C_{x^*} and C_{My^*} or C_{y^*} and C_{Mx^*} respectively, which may occur temporarily at sea.

Apart from these specific cases, tables II and III recap the load extreme values and ranges for several flow conditions with maximal values in red and minimal in green. Typically, the unsteady flow conditions, either due to the bathymetry-generated turbulence or to the presence of large surface waves, are responsible for most of the loads extreme values and ranges. The waves cause maximal values and maximal ranges of the streamwise and vertical loads due to the orbital velocities propagating in the water column. The bathymetry-generated turbulence, for its part, is responsible for the maximal value and range of C_{Mz} among all the tested experimental cases. That load component is the critical one for the design of the base mast structure. We also notice that the maximal transverse loads C_{y^*} and C_{Mx^*} occur when the 2-VATT operates with a misalignment angle of ±15°.

Therefore, a combination of misalignment angle with large surface wave flow conditions and the two rotor

columns in phase would provide the worst situation in terms of load extreme values. That situation must be considered as the ultimate limit state for the structural design of the device as the extreme loads are 1.25 to 2.25 times higher than in the reference idealised flow condition. It would also be the worst case scenario for the design of the base regarding the risks of sliding and overturning. The structural design from the fatigue loads point of view is essentially conditioned by the turbulence and the surface waves as the load ranges are 3 to 10 times larger in these flow conditions compared to the uniform steady flow.

IV. Conclusion

The paper provides a synthesis of the experimental results obtained by testing a 1/20 scale model of *Hydro-Quest*'s 1-MW rated twin vertical axis tidal turbine (2-VATT) demonstrator in a diversity of flow conditions in the Ifremer's wave and current tank. We address the effect of the incident flow shear, of the the relative flow misalignment, of bathymetry obstacles upstream the turbine and of surface waves on both the power performance and the loads of the 2-VATT. The results show that the average power performance is rather insensitive to the incident flow conditions whereas the power and load distributions can be strongly affected. The knowledge enhancement regarding the 2-VATT response to its environment contributes to build confidence in the turbine design methodology and so to drive the production costs down. To keep improving the power performance prediction and the structure design method, a complete comparison between the experimental results at reduced-scale and the full-scale results is ongoing.

Acknowledgement

The authors acknowledge Jean-Valéry Facq and Cédric Derveaux for the design of the turbine model as well as Thomas Bacchetti, Benoît Gomez and Benoît Gaurier for their help during the experiments.

References

[1] IEA-OES, "Annual report: An overview of ocean energy activities in 2022," International Energy Agency, Tech. Rep., 2022. [Online]. Available: https://www.ocean-energy-systems.org/publications/oes-annual-reports/

[2] M. Moreau, G. Germain, G. Maurice, and A. Richard, "Sea states influence on the behaviour of a bottom mounted full-scale twin vertical axis tidal turbine," *Ocean Engineering*, vol. 265, p. 112582, dec 2022.

[3] L. Furgerot, P. B. Du Bois, Y. Méar, M. Morillon, E. Poizot, and A. C. Bennis, "Velocity profile variability at a tidal-stream energy site (Alderney Race, France): From short (second) to yearly time scales," in *OCEANS and MTS/IEEE Kobe Techno-Oceans*. IEEE, 2018, pp. 2779–2789.

[4] P. Mercier and S. S. Guillou, "Spatial and temporal variations of the flow characteristics at a tidal stream power site: A high-resolution numerical study," *Energy Conversion and Management*, vol. 269, no. May, p. 116123, oct 2022.

[5] P. Mercier and S. Guillou, "The impact of the seabed morphology on turbulence generation in a strong tidal stream," *Physics of Fluids*, vol. 33, no. 5, p. 055125, may 2021.

[6] A.-C. Bennis, L. Furgerot, P. Bailly Du Bois, E. Poizot, Y. Méar, and F. Dumas, "A winter storm in Alderney Race: Impacts of 3D wave–current interactions on the hydrodynamic and tidal stream energy," *Applied Ocean Research*, vol. 120, no. December 2021, p. 103009, 2022.

[7] M. Magnier, N. Delette, P. Druault, B. Gaurier, and G. Germain, "Experimental study of the shear flow effect on tidal turbine blade loading variation," *Renewable Energy*, p. 100061, may 2022.

[8] P. K. Modali, A. Vinod, and A. Banerjee, "Towards a better understanding of yawed turbine wake for efficient wake steering in tidal arrays," *Renewable Energy*, vol. 177, pp. 482–494, 2021.

[9] B. Gaurier, M. Ikhennicheu, G. Germain, and P. Druault, "Experimental study of bathymetry generated turbulence on tidal turbine behaviour," *Renewable Energy*, vol. 156, pp. 1158–1170, 2020.

[10] S. Draycott, J. Steynor, A. Nambiar, B. Sellar, and V. Venugopal, "Rotational sampling of waves by tidal turbine blades," *Renewable Energy*, vol. 162, pp. 2197–2209, 2020.

[11] V. F. Rolin and F. Porté-Agel, "Experimental investigation of vertical-axis wind-turbine wakes in boundary layer flow," *Renewable Energy*, vol. 118, pp. 1–13, apr 2018.

[12] E. E. Lust, B. H. Bailin, and K. A. Flack, "Performance characteristics of a cross-flow hydrokinetic turbine in current only and current and wave conditions," *Ocean Engineering*, vol. 219, p. 108362, jan 2021.

[13] M. Moreau, G. Germain, and G. Maurice, "Experimental performance and wake study of a ducted twin vertical axis turbine in ebb and flood tide currents at a 1/20th scale," *Renewable Energy*, vol. 214, pp. 318–333, sep 2023.

[14] ——, "Misaligned sheared flow effects on a ducted twin vertical axis tidal turbine," *Applied Ocean Research*, vol. 138, p. 103626, sep 2023.

[15] M. Moreau, N. Bloch, G. Maurice, and G. Germain, "Experimental study of the upstream bathymetry effects on a ducted twin vertical axis tidal turbine," *Renewable Energy (Under review)*, 2023.

[16] M. Moreau, G. Germain, and G. Maurice, "Experimental investigation of surface waves effect on a ducted twin vertical axis tidal turbine," *In preparation*, 2023.

[17] B. Gaurier, G. Germain, J.-V. Facq, and T. Bacchetti, "Wave and current flume tank of IFREMER at Boulogne-sur-mer. Description of the facility and its equipment," IFREMER, Tech. Rep., 2018.

[18] N. Bloch, M. Moreau, G. Germain, and G. Maurice, "Experimental study of bathymetry variation effects on a cross-flow water turbine," in *18èmes Journées de l'Hydrodynamique*, Poitiers, 2022, pp. 1–12. [Online]. Available: https://jh2022.sciencesconf.org/413851

[19] Y. Saouli, M. Magnier, G. Germain, B. Gaurier, and P. Druault, "Experimental characterisation of the waves propagating against current effects on the wake of a wide bathymetric obstacle," in *18ème Journées de l'Hydrodynamique*, no. 1, Poitiers, 2022, pp. 1–12. [Online]. Available: https://jh2022.sciencesconf.org/413878

[20] B. Gaurier, "Etude expérimentale des performances d'une hydrolienne, soumise aux effets de la turbulence et de l'intéraction houle-courant," Ph.D. dissertation, Normandie Université, nov 2020. [Online]. Available: https://tel.archives-ouvertes.fr/tel-03030615

[21] M. Ikhennicheu, G. Germain, P. Druault, and B. Gaurier, "Experimental study of coherent flow structures past a wall-mounted square cylinder," *Ocean Engineering*, vol. 182, no. May, pp. 137–146, jun 2019.

[22] M. Magnier, P. Druault, and G. Germain, "Experimental investigation of upstream cube effects on the wake of a wall-mounted cylinder: Wake rising reduction, TKE budget and flow organization," *European Journal of Mechanics - B/Fluids*, vol. 87, no. June, pp. 92–102, may 2021.

[23] J. Michna and K. Rogowski, "Numerical Study of the Effect of the Reynolds Number and the Turbulence Intensity on the Performance of the NACA 0018 Airfoil at the Low Reynolds Number Regime," *Processes*, vol. 10, no. 5, p. 1004, may 2022.

[24] P. Bachant and M. Wosnik, "Effects of Reynolds Number on the Energy Conversion and Near-Wake Dynamics of a High Solidity Vertical-Axis Cross-Flow Turbine," *Energies*, vol. 9, no. 2, p. 73, jan 2016.